Int. J. Heat Mass Transfer. Vol. 34, No. 3, pp. 693–702, 1991
Printed in Great Britain

0017–9310/91 $3.00 + 0.00
Pergamon Press plc

Free convection heat transfer of air–water layers in a horizontal cooled circular tube

S. FUKUSAKO and M. TAKAHASHI
Department of Mechanical Engineering, Hokkaido University, Sapporo 060, Japan

(*Received* 8 *January* 1990 *and in final form* 16 *April* 1990)

Abstract—The influence of density inversions and free convection heat transfer of air–water layers in a horizontal tube with uniformly decreased wall temperature is investigated. Holographic interferometry is adopted to determine the time-dependent temperature distribution in the tube. The temperature and the flow patterns are markedly influenced by the cooling rate of the tube. The heat transfer characteristics along the tube wall are also determined. It is found that there are three characteristic dendritic ice growth patterns starting from the air–water interface, and also pure ice growth along the tube wall.

1. INTRODUCTION

FREEZING water generating latent heat is a widely observed phenomenon in freezing environments. This phenomenon is utilized in ice manufacture, frozen foods, and ice-accumulation systems. However, freezing often causes deterioration or destruction of heat exchangers, industrial pipes, etc. In cold regions, it also results in the fracture of water and sewer pipes. Freezing easily occurs when there is no main flow through a pipe.

A number of studies [1–6] have investigated the freezing characteristics and free convection of water. Gilpin [6] studied the cooling of a horizontal water cylinder with wall temperatures decreasing at constant rates through the maximum density point at 4°C, and found four flow regimes: transient, quasi-steady, inversion, and quasi-steady states, before freezing. He also made an approximate theoretical analysis with a quasi-steady boundary-layer model. A theoretical analysis by Cheng and Takeuchi [5] investigated the transient natural convection of water in a horizontal pipe with constant cooling rates through 4°C. The results were in general agreement with those of Gilpin's [6] quasi-steady boundary-layer model and discussed implications on the subsequent freezing process.

Gilpin [2, 3] studied dendritic ice when water and the pipe wall were at a uniform temperature at ice nucleation. Here the dendritic ice growth occurs only in supercooled water and does not result in pipe blockage as the extent of the dendritic ice growth is determined by the temperature distribution at ice-nucleation time. These studies used tubes that were filled with water. There is no study of the freezing characteristics of layered air and liquid phases in a circular tube.

This paper investigates the free convection heat transfer of air–water layers and the dendritic ice nucleation within a cooled circular tube. The experiments were carried out at different cooling rates and water levels in the tube. Holographic interferometry was adopted to determine the time-dependent temperature distribution in the tube. The time-dependent sequential flow patterns were observed and the heat transfer characteristics experimentally determined.

2. EXPERIMENTAL APPARATUS AND PROCEDURES

2.1. *Experimental apparatus*

The experimental apparatus consists of a test section and an optical system. Details of the test section are shown in Fig. 1. The test section is a composite tube with an inner 1.5 mm thick copper tube of 65 mm o.d. The outer tube is a 5 mm thick vinyl chloride pipe with a 165 mm o.d. Both ends of the composite tube are closed with a pair of Plexiglas flanges with an air gap to accommodate the laser beam and to enable observation inside the tube.

The copper tube was covered by 1 mm thick teflon sheets arranged at 0.5 mm intervals along the tube wall and bound tightly by 50 μm thick copper foil. The temperatures of the copper-tube wall and water were determined with 0.1 mm diameter C–A thermocouples installed at 30° intervals at both the inside and outside of the teflon sheets, and at 15° intervals near the air–water interface. To ensure a uniform temperature of the copper-tube wall, temperature-controlled brine was injected along the copper tube from 12 nozzles at regular intervals.

A holographic interferometry technique was adopted to measure the temperature distribution in the tube. Observations of the sequential flow patterns were performed by a tracer method using aluminum powder. The laser beam was from a He–Ne gas laser (500 mV).

2.2. *Experimental procedures*

The optical apparatus (see Fig. 2) was set up to measure the temperature distribution in the test section by real-time holographic interferometry. First.

NOMENCLATURE

C_p	specific heat [kJ kg^{-1} K^{-1}]
D	diameter of tube [m]
g	acceleration of gravity [m s^{-2}]
H	water level [m]
h_ϕ	local heat transfer coefficient, $q_\phi/(T_{H/2}-T_w)$ [W m^{-2} K^{-1}]
L	length of tube [m]
Nu_ϕ	local Nusselt number, $h_\phi H/\lambda$
q_ϕ	local heat flux [W m^{-2}]
q_m	average heat flux [W m^{-2}]
T	temperature [°C]
T_f	freezing temperature [°C]
$T_{H/2}$	water-layer temperature halfway between bottom of tube and water level or air-layer temperature halfway between water surface and top of tube [°C]
T_w	tube wall temperature [°C]
t	time [min or s]
t_c	time of dendritic ice growth [min or s]
V	volume [m^3].

Greek symbols

θ_v	cooling rate [°C min^{-1}]
λ	thermal conductivity [W m^{-1} K^{-1}]
ρ	density [kg m^{-3}]
ϕ	angle from top of tube (clockwise) [deg].

Subscripts

c	copper tube wall
t	teflon
ini	initial value.

the optical axis was adjusted to make the optical path difference between the reference waves less than 100 mm, and the laser beam was changed into a collimator wave by the object lens. To make the signal wave coincide with the reference wave on the dry plate the optical axis was further adjusted. The luminous intensity ratio was controlled by the ND filter to make the signal wave to reference wave ratio approximately one-tenth. Then pure water was poured into the test section and the water level H was set at 16, 32 or 48 mm. The basic holograph was made with the water temperature in the tube at 5°C. The development and fixation of this hologram were practised in the liquid gate.

To ensure uniform temperature of the copper-tube wall, brine was injected from 12 nozzles arranged at identical intervals (see Fig. 1). The tube-wall temperature was decreased linearly with time until dendritic ice formation in the pipe. Observations of the sequential flow pattern in the pipe were performed by aluminum powder tracer particles. The light source for the test section was a He–Ne gas laser.

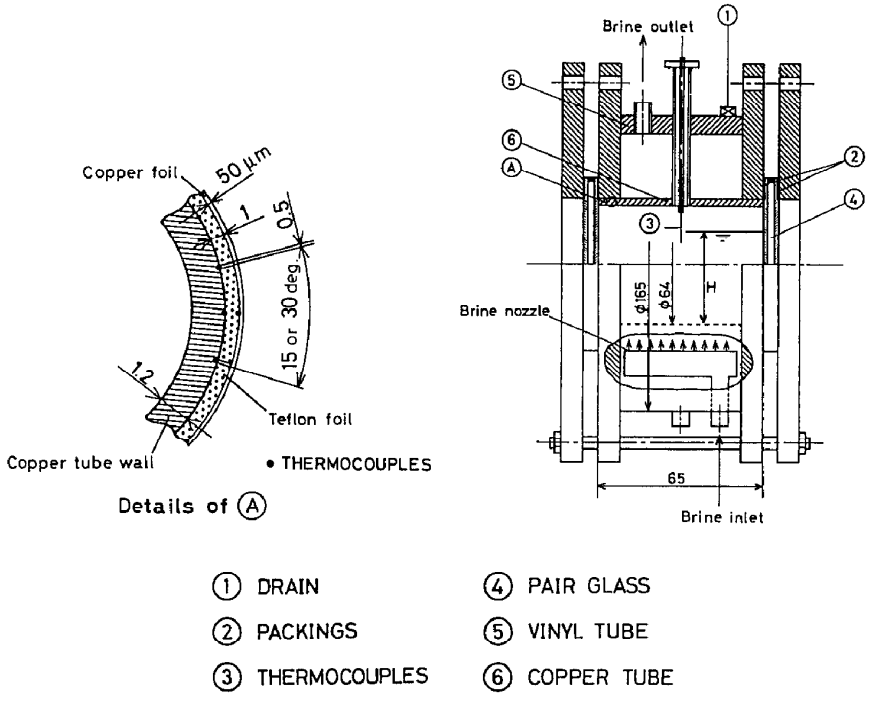

FIG. 1. Test section.

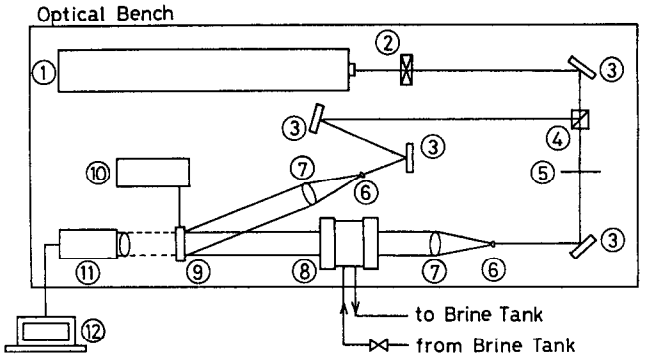

① He-Ne GAS LASER ⑤ ND FILTER ⑨ LIQUID GATE
② SHUTTER ⑥ OBJECT LENS ⑩ FLOAT TANK
③ MIRROR ⑦ COLLIMATOR LENS ⑪ TV CAMERA
④ BEAM SPLITTER ⑧ TEST SECTION ⑫ CALCULATOR

FIG. 2. Optical set-up for real-time holographic interferometry.

2.3. *Estimating the local heat flux along the tube*

The local heat flux was assessed from the temperature difference between the inside and outside of the teflon sheets on the copper-tube wall. Considering the heat capacity of the teflon sheets and the copper tube, the heat flux may be expressed as

$$q_\phi = \lambda_t \Delta T_t/\Delta r - (\rho_t V_t C_{pt} \Delta T_t + \rho_c V_c C_{pc} \Delta T_c)/(\pi D L \Delta t) \quad (1)$$

where ΔT_t is the mean-temperature difference between the inside and outside of the teflon sheets during the time Δt. The total heat flow was also estimated from the temperature difference between the brine inlet and outlet, considering the heat capacity of the test section (copper tube, vinyl-chloride pipe, and lucite plate).

Figure 3 shows the mean values of the local heat flux evaluated from equation (1) and the difference between the inlet and outlet temperature of the brine for $H = 48$ mm, $T_{ini} = 5.0°C$, and $\theta_v = 0.27°C\ min^{-1}$. It is revealed in the figure that there is agreement within about $\pm 5\%$ between equation (1) and the measured total heat flux.

3. RESULTS AND DISCUSSION

3.1. *Temperature distribution and flow pattern*

Figure 4 shows the temperature distribution (a), photographs of time-dependent sequential flow pat-

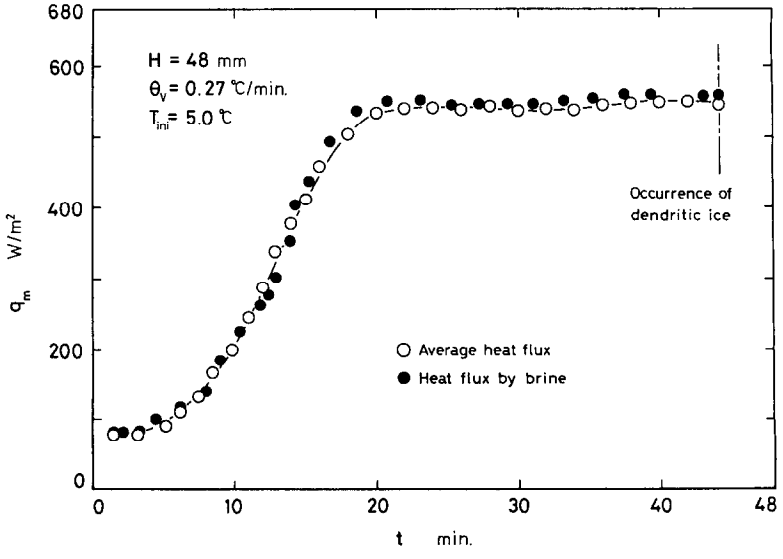

FIG. 3. Average heat flux in tube.

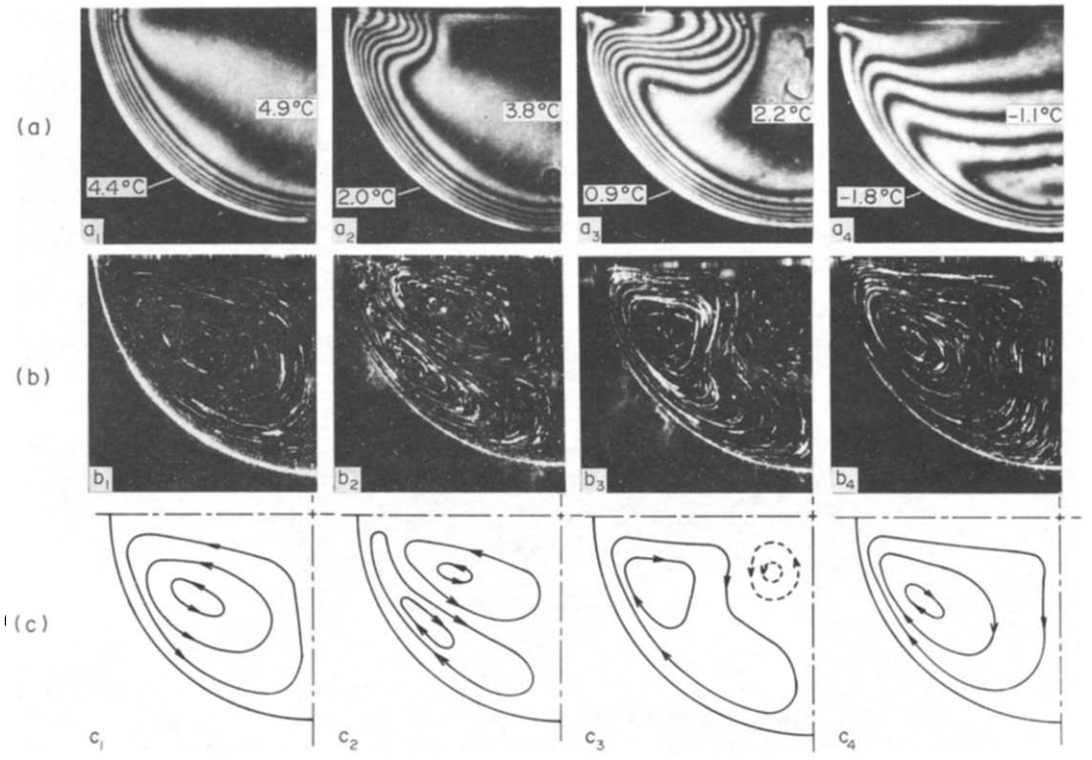

FIG. 4. Interferograms and flow patterns: 1, 1 min; 2, 11 min; 3, 15 min; 4, 25 min elapsed.

terns (b), and a schematic diagram of flow patterns (c) in the circular tube for $\theta_v = 0.27$°C min^{-1} and $T_{ini} = 5.0$°C. Figure 5 shows transient distributions of wall temperature, centerline temperature for the water layer, and centerline temperature for the air layer. It seems that the wall temperature is decreased linearly as the time elapses.

One minute from the start of the experiment, there are dense interference rings near the tube wall (a), possibly due to the thermal boundary layer along the wall. At this time, the water temperature near the tube wall is above 4°C and cooled water flows down along the tube wall, and the streamlines form a counter-clockwise eddy (c_1) as the water density increases with decreasing water temperature (see Fig. 6). After 11 min, the interference rings move from the edge of the air–water interface to the center of the tube (a_2), and there is both a clockwise and a counter-clockwise eddy (b_2, c_2). This two eddy phenomenon may be due to density inversion in the water. The water temperature is below 4°C and water ascends along the tube wall and creates a clockwise flow near the air–water interface. As a result the cooled water moves from the edge of the air–water interface towards the center of the tube by convection. At 15 min, the clockwise secondary eddy has enlarged, and the counter-clockwise eddy is disappearing (b_3). The interference rings reach further from the edge of the air–water interface towards the center of the tube (c_3). The figure shows that the air–water interface is initially supercooled.

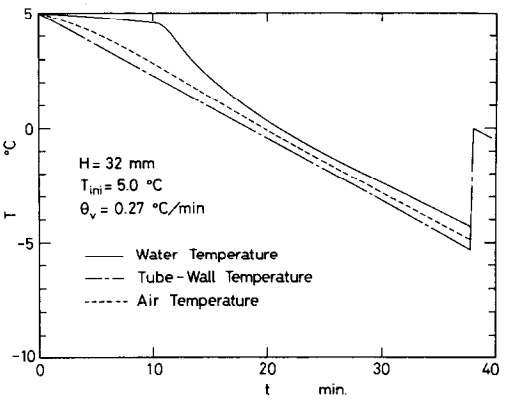

FIG. 5. Transient distribution of tube-wall temperature and centerline temperatures in air and water layers.

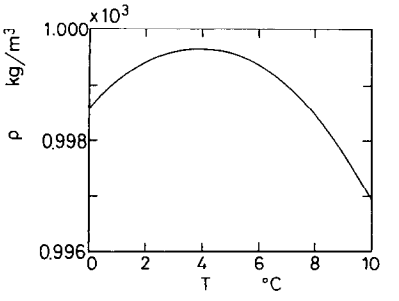

FIG. 6. Relationship between water density and temperature.

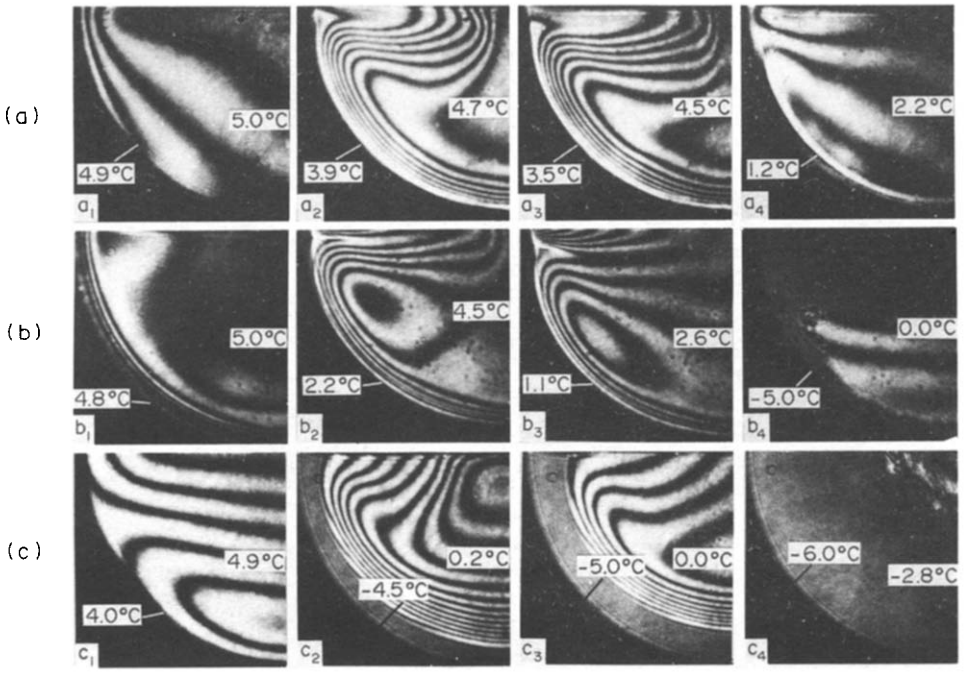

FIG. 7. Interferograms for cooling rate: 1, 30 s; 2, 10 min; 3, 14 min; 4, 37 min elapsed.

After 25 min, the interference rings have spread throughout the tube. The water temperature has dropped below 4°C, and only the clockwise eddy remains.

3.2. *Effect of cooling rate on temperature-distribution characteristics*

Figure 7 shows the temperature in the tube obtained by a hologram for an initial water temperature of $T_{ini} = 5.0$°C and a cooling rate of 0.10, 0.27, and 3.87°C min^{-1}. In Fig. 7(a) ($\theta_v = 0.10$°C min^{-1}), the interference rings spread from the edge of the air–water interface to the center in 10 min (a_2). The interference ring is isothermal and there is a decrease in water temperature due to heat discharge from the tube wall. After 14 min (a_3), the interference rings have migrated to the middle of the tube. From here they spread out toward the tube bottom, and after 37 min the temperature distribution in the tube becomes almost uniform.

In Fig. 7(b) ($\theta_v = 0.27$°C min^{-1}), the interference rings have reached the middle of the tube after 10 min as the cooling rate is higher than in Fig. 7(a). After 14 min the interference rings have reached the bottom of the tube. After 37 min (b_4), dendritic ice is observed at the air–water interface where the water temperature has been cooled below the fusion temperature. Figure 7(c) demonstrates the temperature distribution for a higher cooling rate ($\theta_v = 3.87$°C min^{-1}). After 30 s (c_1), rings already distribute throughout the tube as the cooling rate is quite large. After 10 min the interference rings have reached the center of the tube, and ice has formed along the tube wall (c_2). This ice keeps growing, and the tube is almost filled with the ice after 37 min of cooling (c_4). Under this experimental condition, there was no dendritic ice formation.

3.3. *Effect of cooling rate on local heat flux in a tube*

Figures 8(a) and (b) show the local heat flux of the water side (○) and the air side (□) for $H = 32$ mm, $T_{ini} = 5.0$°C at $\theta_v = 0.65$ and 0.10°C min^{-1}, respectively. In Fig. 8(a), the local heat flux rapidly increases until 9 min (when density inversion occurs) as the cooling rate is large ($\theta_v = 0.65$°C min^{-1}). At $\phi = 97°$ (at the edge of the air–water interface) the local heat flux decreases slightly and then increases until dendritic ice appears after 21 min of cooling. The heat

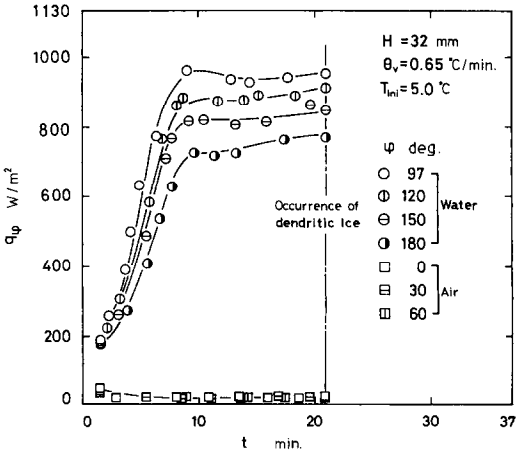

FIG. 8(a). Local heat flux.

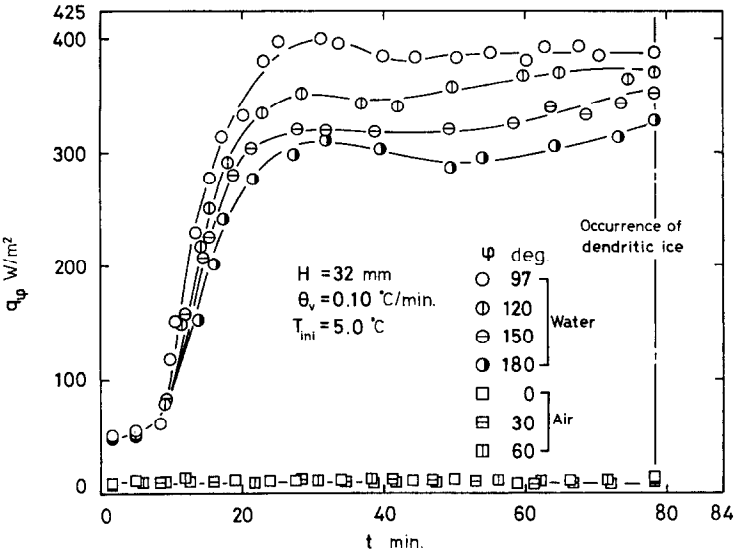

FIG. 8(b). Local heat flux.

flux increases slightly except at $\phi = 97°$. In addition, the value of the local heat flux decreases with increasing degree.

The above-mentioned phenomena are possibly due to the following fact. The water is cooled rapidly near the tube wall as the cooling rate is high ($\theta_v = 0.65°C\ min^{-1}$) and the influence of the clockwise eddy increases with time. The increase in local heat flux is small as the clockwise secondary eddy, which is due to the density inversion after 9 min, reduces the influence of the counter-clockwise eddy. As the influence of this secondary eddy increases with time, the change in the local heat flux spreads slowly from the edge of the air–water interface to the bottom of the tube. The bottom corresponds to a stagnation point and the heat flux at the bottom is lower than at the edge of the air–water interface. The local heat flux is gradually increasing from the edge of the air–water interface to the bottom.

Figure 8(a) also shows the local heat flux at the air side. Both the absolute value and variation of the heat flux are very small, as expected.

Figure 8(b) shows changes in the local heat flux for a low cooling rate ($\theta_v = 0.10°C\ min^{-1}$). The local heat flux increases with time and reaches a maximum after 28 min, lower than with the high cooling rate (see Fig. 8(a), $\theta_v = 0.65°C\ min^{-1}$). Except at the air–water interface ($\phi = 97°$), the local heat flux then decreases before it recovers slightly. Dendritic ice occurs at about 78 min later than for smaller cooling rates. This is explained as follows. (1) With low cooling rates the temperature differences in the water near the tube wall and the influence of the eddy are small. (2) Cooling is slow and both the secondary eddy and the dendritic ice formations are late. The heat flux along the tube wall in the air layer decreases only slightly with the cooling rate.

3.4. *Effect of cooling rate on local Nusselt number*

The local heat transfer coefficient was assessed based on the assumptions that: (1) the reference temperature in the water layer is in the middle of the water (on the centerline of the tube); (2) the reference temperature in the air layer is defined halfway between the water surface and the top of the tube (on the centerline of the tube). The value of the heat flux calculated by equation (1) is divided by the difference between the reference temperature and the tube-wall temperature to determine the Nusselt number. The water- and air-side reference lengths are defined as the distance between the water surface and the top or bottom of the tube. The thermophysical properties were calculated at the reference temperatures in the air and water.

Figures 9(a) and (b) demonstrate the time-dependent sequential Nusselt number for $\theta_v = 0.65$ and

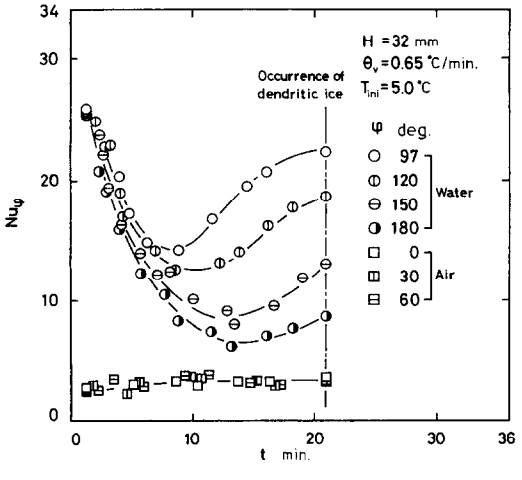

FIG. 9(a). Local Nusselt number.

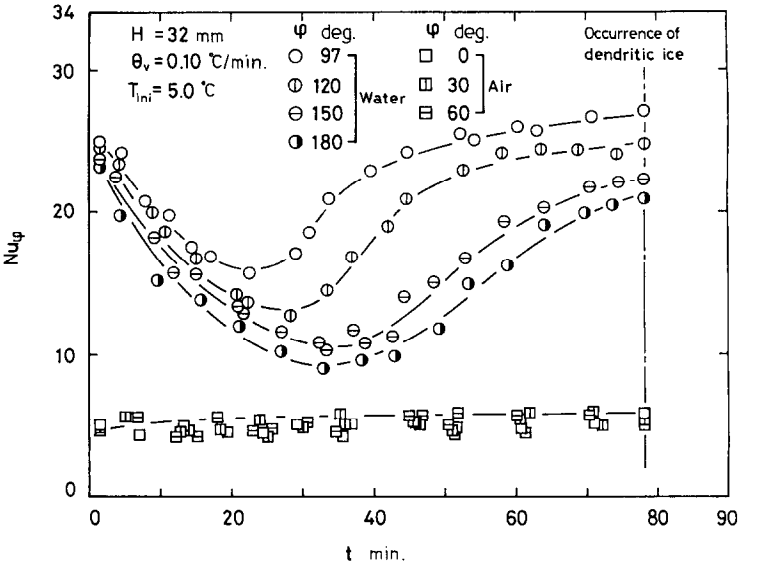

FIG. 9(b). Local Nusselt number.

0.1°C min^{-1}, respectively. The ordinate denotes the local Nusselt number, while the abscissa denotes the time. In Fig. 9(a), the local Nusselt number decreases abruptly with time when the cooling rate is large ($\theta_v = 0.65$°C min^{-1}). The local Nusselt number at the edge of the air–water interface ($\phi = 97°$) reaches a minimum after 9 min of operation and at the bottom ($\phi = 180°$) after 11 min. The local Nusselt number increases rapidly at the air–water interface ($\phi = 97°$) until dendritic ice appears after 21 min, and its growth changes from the air–water interface to the bottom of the tube. As mentioned in Section 3.3, this may be attributed to the following: when the cooling rate is large, the water near the tube wall is cooled rapidly, then (1) the appearance of the secondary eddy is earlier, (2) the influence of the original eddy drops off quickly, and (3) the increase in the secondary eddy becomes large.

Figure 9(b) shows the results for the low cooling rate, $\theta_v = 0.10$°C min^{-1}. The local Nusselt number decreases, but the decrease is smaller than at the high cooling rate ($\theta_v = 0.65$°C min^{-1}). The Nusselt number reaches the minimum after 19–27 min as the secondary eddy appears and thus the dendritic ice growth is late. After the minimum, the increase occurs from the bottom of the tube ($\phi = 180°$) to the edge of the air–water interface ($\phi = 97°$), and the rate of increase is smaller than for the high cooling rate ($\theta_v = 0.65$°C min^{-1}). With increasing cooling rate, the differences between the Nusselt number at the air–water interface ($\phi = 97°$) and the bottom ($\phi = 180°$) of the tube also increases. This is attributed to the fact that the water in the tube is cooled gradually at the low cooling rate and then dendritic ice growth starts after supercooled water has spread to the whole tube. The local Nusselt number in the air layer generally increases at a very low rate with decreasing cooling rate.

3.5. *Effect of water level on local Nusselt number*

Figure 10(a) shows the Nusselt numbers for $T_{ini} = 5.0$°C, and $\theta_v = 0.10$°C min^{-1} for $H = 48$ mm and Fig. 10(b) for $H = 16$ mm. For $H = 48$ mm the local Nusselt number reaches the minimum value about 20–30 min into the experiment, later than at $H = 32$ mm (Fig. 9(b): 19–27 min). Dendritic ice also appears later for $H = 48$ mm than for $H = 32$ mm (Fig. 9(b)) (see Fig. 10(b): after about 69 min, and Fig. 10(a): after about 103 min). The difference between local Nusselt number at the air–water interface and the tube bottom just before the dendritic ice growth appears, increases with increasing water level. This may be due to the longer time it takes to cool the large amount of water in the tube, and because the temperature difference between the air–water interface and the bottom of the tube becomes larger.

In Fig. 10(b) ($H = 16$ mm) the local Nusselt number reaches a minimum value due to the appearance of the secondary eddy at 17–20 min, earlier than for $H = 48$ (Fig. 10(a)) and 32 mm (Fig. 9(b)). After the minimum the increase in Nusselt number is smaller than at $H = 48$ and 32 mm. The reason maybe that the circulation of the secondary eddy is retarded by surface-tension forces at the air–water interface. Dendritic ice growth starts earlier (at about 69 min) than for $H = 48$ and 32 mm, and the difference in the local Nusselt number between the air–water interface and tube bottom just before the appearance of the dendritic ice is smaller. Though surface tension acts as the water in the tube is cooled, this may be explained by the water being sufficiently supercooled due to the low cooling rate. In Figs. 10(a) and (b), the local

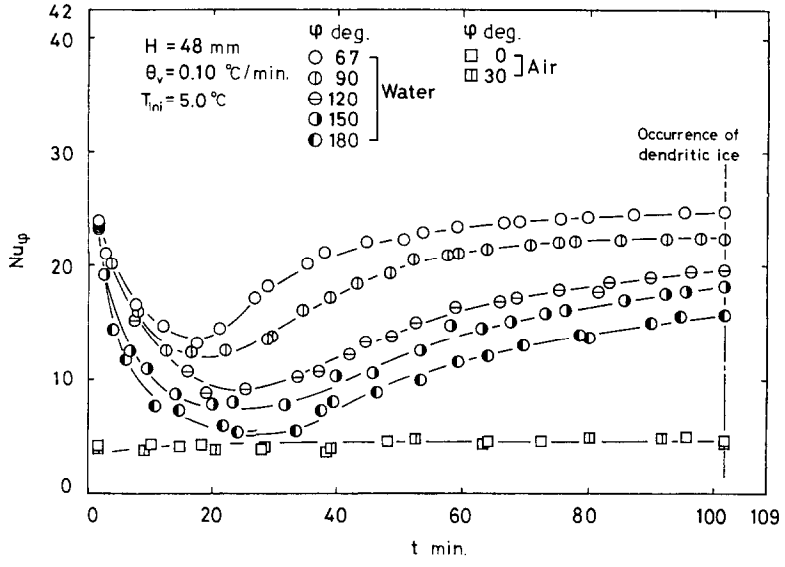

FIG. 10(a). Local Nusselt number.

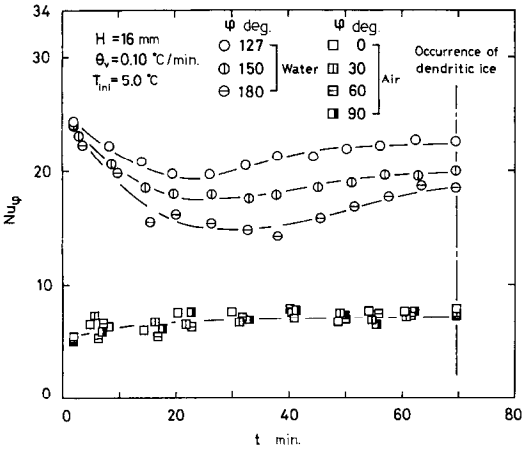

FIG. 10(b). Local Nusselt number.

Nusselt number of the air layer decreases slightly with increasing water level, while its ratio of decrease is quite small.

3.6. *Occurrence of dendritic ice and classification of its distribution*

Figure 11 shows the characteristics of dendritic ice growth for $T_{ini} = 5.0°C$, $H = 32$ mm, and $\theta_v = 0.27°C$ min^{-1}. At 37 min and 56.04 s (1) into the experiment, the dendritic ice starts to form from the edge of the air–water interface. A second later (37 min 57.09 s (2)) it starts spreading towards the tube bottom, and at 37 min 58.12 s (3) there is thick dendritic ice in the water. The dendritic ice growth is sudden after the water has supercooled considerably ($-4 \sim -8°C$). The supercooling disappears when the dendritic ice appears, and the temperature of the remaining water returns to 0°C instantaneously, as latent heat is released by the ice growth.

The distribution of dendritic ice in the tube changes with the cooling rate, and Fig. 12 shows dendritic ice growth characteristics for $\theta_v = 0.10$, 0.80, and 2.00°C min^{-1}. In Fig. 12(a) ($\theta_v = 0.10°C$ min^{-1}), the dendritic ice spreads into all the water within 1 or 2 s. At $\theta_v = 0.80°C$ min^{-1} (b), sherbet-like ice forms just below the water surface, and the ice grows towards the bottom of the tube. At the highest cooling rate ($\theta_v = 2.00°C$ min^{-1} (c)), the dendritic ice does not spread to the whole air–water interface.

Figure 13 classifies characteristics of dendritic ice which spreads from the edge of the air–water interface. The ordinate shows the time since the start of cooling t_c, when the dendritic ice appears, and the abscissa is the cooling rate θ_v. The regions (A), (B) and (C) correspond to the dendritic ice shown in Figs. 12(a)–(c), respectively. There is no dendritic ice in region (D), while pure ice grows along the tube wall below the water surface. Figure 13 shows that the time of appearance of dendritic ice growth is not affected by changes in the water level, but varies with the cooling rate.

4. CONCLUSIONS

Free convection heat transfer of air–water layers in a horizontal cooled circular tube was investigated, and the following summarizes the results:

(1) Initially cooled water in the tube flows downward along the tube wall. Next a secondary eddy is formed due to density inversion in the water, and it flows upward along the tube wall, while the initial downward flowing eddy becomes weaker and finally disappears.

(2) The water at the air–water interface is supercooled by the density inversion, and this supercooled

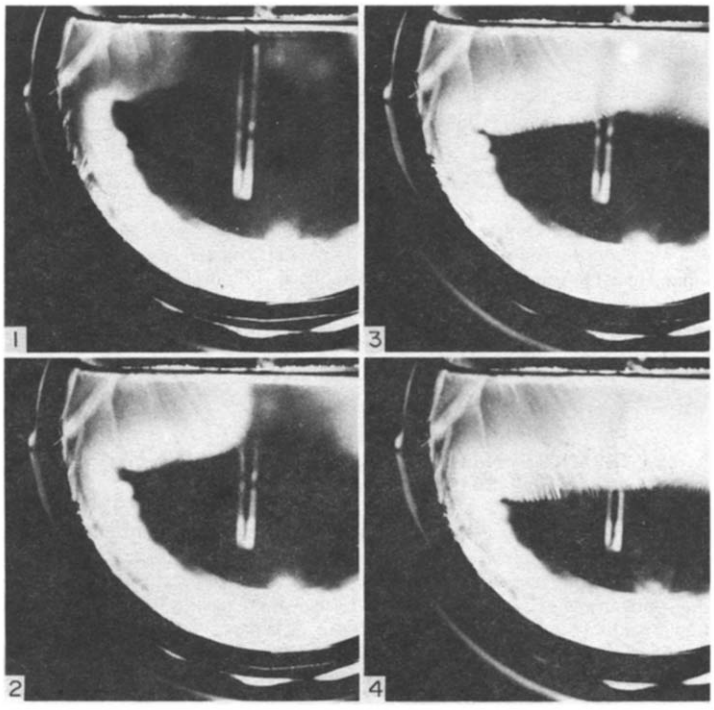

FIG. 11. Dendritic ice formation.

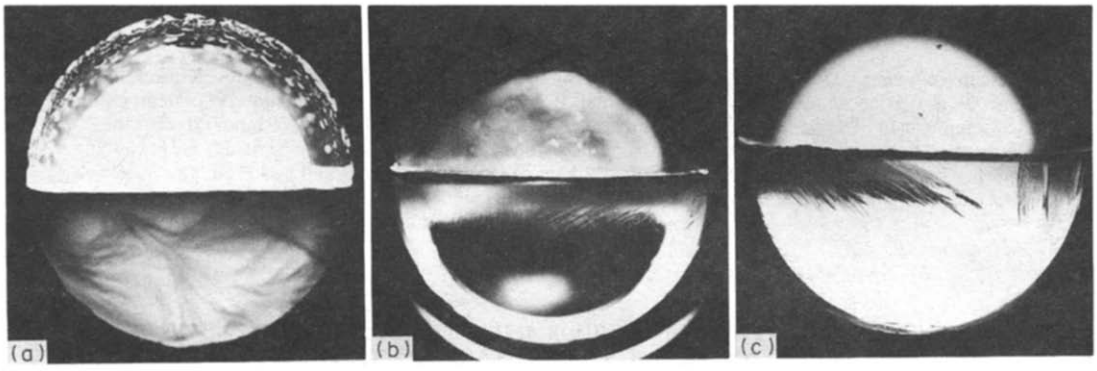

FIG. 12. Characteristics of dendritic ice.

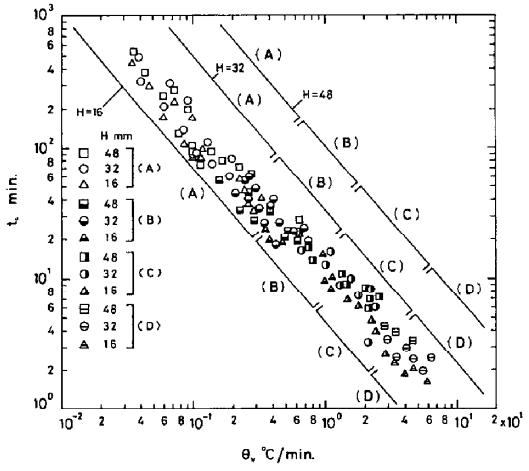

FIG. 13. Classification of dendritic ice growth.

water gradually spreads to the tube bottom by free convection.

(3) The local heat flux increases with the cooling rate until the secondary eddy appears. The local heat flux on the air layer increases with the cooling rate, but the rate of increase is very small during the experiment.

(4) With higher cooling rates, the local minimum Nusselt number and dendritic ice appear earlier. The difference in the local Nusselt number just before dendritic ice appears between the air–water interface and the tube bottom becomes larger.

(5) The local Nusselt number in the air layer increases slightly with both decreasing cooling rate and decreasing water level.

(6) The distribution of dendritic ice varies with cooling rate. There are three different regions with

characteristic dendritic ice formation and a region without dendritic ice.

Acknowledgements—The authors wish to thank Mr Y. Wada and Mr N. Yamashita for their help in the experiments.

REFERENCES

1. S. Fukusako, Y. Wada and N. Yamashita, Free convection heat transfer of air–water layers in a cooled circular cylinder, 23rd Japan Heat Transfer Symp., pp. 379–402 (1983).
2. R. R. Gilpin, The effect of dendritic ice formation in water pipes, *Int. J. Heat Mass Transfer* **20,** 693–699 (1977).
3. R. R. Gilpin, The effect of cooling rate on the formation of dendritic ice in a pipe with no main flow, *Trans. ASME J. Heat Transfer* **99,** 419–424 (1977).
4. T. Kashiwagi, S. Hirose, S. Itoh and Y. Kurosaki, Effect of natural convection in a partially supercooled water cell on the release of supercooling, *Trans. JSME* **53,** 1822–1827 (1987).
5. K. C. Cheng and M. Takeuchi, Transient natural convection of water in a horizontal pipe with constant cooling rate through 4°C, *Trans. ASME J. Heat Transfer* **98,** 581–587 (1976).
6. R. R. Gilpin, Cooling of a horizontal cylinder of water through its maximum density point at 4°C, *Int. J. Heat Mass Transfer* **18,** 1307–1315 (1975).

CONVECTION THERMIQUE NATURELLE DE COUCHES AIR EAU DANS UN TUBE CIRCULAIRE HORIZONTAL REFROIDI

Résumé—On étudie l'influence de l'inversion de densité et la convection thermique naturelle de couches air–eau dans un tube horizontal soumis à une température pariétale uniformément décroissante. On utilise l'interférométrie holographique pour déterminer la distribution de température variable dans le temps. La température et les configurations de l'écoulement sont fortement influencées par la vitesse de refroidissement du tube. Les caractéristiques du transfert thermique le long de la paroi du tube sont déterminées. On trouve qu'il y a trois configurations caractéristiques de croissance dendritique de la glace à partir de l'interface air–eau, et aussi une croissance de glace pure sur la paroi du tube.

WÄRMEÜBERGANG DURCH FREIE KONVEKTION IN EINER LUFT/WASSER-SCHICHT IN EINEM WAAGERECHTEN GEKÜHLTEN KREISROHR

Zusammenfassung—Der Einfluß der Dichteinversion und des Wärmeübergangs durch freie Konvektion in einer Luft/Wasser-Schicht in einem waagerechten Rohr mit gleichförmig abnehmender Wandtemperatur wird untersucht. Die zeitabhängige Temperaturverteilung im Rohr wird mittels holografischer Interferometrie bestimmt. Temperatur und Strömungsformen werden von der Intensität der Rohrkühlung spürbar beeinflußt. Außerdem wird der Wärmeübergang entlang der Rohrwand bestimmt. Es zeigen sich drei charakteristische Wachstumsformen von Eis-Dendriten an der Luft/Wasser-Grenzfläche. Auch reines Eiswachstum an der Rohrwand kommt vor.

СВОБОДНОКОНВЕКТИВНЫЙ ТЕПЛООБМЕН В ВОЗДУШНО-ВОДЯНЫХ СЛОЯХ ВНУТРИ ОХЛАЖДАЕМОЙ ГОРИЗОНТАЛЬНОЙ КРУГЛОЙ ТРУБЫ

Аннотация—Исследуются инверсии плотности и свободноконвективный теплообмен в воздушно-водяных слоях внутри горизонтальной трубы с равномерно убывающей температурой стенки. Для определения нестационарного распределения температуры в трубе использовалась голографическая интерферометрия. Температура и режимы течения существенно зависят от интенсивности охлаждения трубы. Определены также характеристики теплопереноса вдоль трубы. Обнаружены три характерных картины роста дендщитного льда на поверхности раздела между воздухом и водой, а также рост чистого льда вдоль стенки трубы.